Title
Enhanced Ultraviolet Photon Capture in Ligand-Sensitized Nanocrystals

Journal
ACS Photonics, 3(4)

ISSN
2330-4022

Authors
Agbo, Peter
Xu, Tao
Sturzbecher-Hoehne, Manuel
et al.

Publication Date
2016-04-20

DOI
10.1021/acsphotonics.6b00118

Peer reviewed

Enhanced Ultraviolet Photon Capture in Ligand-Sensitized Nanocrystals

Peter Agbo,[†] Tao Xu,[‡] Manuel Sturzbecher-Hoehne,[†] Rebecca J. Abergel*[,†]

[†]Chemical Sciences Division and [‡]Material Sciences Division

Lawrence Berkeley National Laboratory

Berkeley, CA 94720, USA

*corresponding author

Abstract

The small absorption cross-sections ($\varepsilon < 10\ M^{-1}\ cm^{-1}$) characteristic of Laporte-forbidden transitions in the f-elements have limited the practical implementation of lanthanide nanoparticles in solar capture devices. While various strategies designed to circumvent the problems of low f-f oscillator strengths have been investigated, comparatively little work has explored the utility of organic ligands with high absorption coefficients ($\varepsilon \sim 10^3$-$10^5\ M^{-1}\ cm^{-1}$) in sensitizing excited states in lanthanide nanocrystals. Here, we detail the photophysics of $NaGd_{1-x}Eu_xF_4$ nanoparticles featuring surface display of the ligand 3,4,3-LI(1,2-HOPO), an aromatic antenna functioning as the terminal light absorber in this system. The result is a ligand-nanocrystal hybrid which converts UV (250-360 nm) light into red Eu(III) luminescence with an external quantum yield of 3.3%. We analyze this sensitization process, responsible for a 10^4 fold increase in luminescence relative to metal-centered excitation, through a quantitative treatment of energy transfer between ligand and metal states.

Keywords: sensitization, lanthanide, ligand antenna, energy transfer, nanocrystal.

The problem of spectral mismatch between semiconductor band gaps and Earth's terrestrial solar spectrum remains an issue plaguing the efficiency of modern photovoltaics[1,2]. A number of methods have been proposed and implemented to address this problem, including the incorporation of materials absorbing at different wavelengths in multi-junction photovoltaics, modification of the intrinsic Si band gap through advanced nanofabrication methods, and the respective up- and down-conversion of low- and high-frequency EM radiation into photons suited for bulk Si absorption[3–6].

Currently, research in the field of spectral conversion is dominated by lanthanide photophysics, where exploitation of f-element nanocrystals has resulted in a wide array of potential downconverters[7–12]. However, the maturation of these prototype systems into practical applications has largely been hampered by the low molar absorptivities of f-f transitions (< 10 M^{-1} cm^{-1})[13,14]. Routes previously explored to address this challenge include the relaxation of Laporte selection rules through the embedding of lanthanide ions in low-symmetry crystal hosts and the employ of parity-allowed, d → f charge transfer in divalent lanthanides such as Eu(II)[15]. By contrast, the possibility of photosensitizing nanocrystalline lanthanides with organic ligands remains a relatively novel method of enhancing f-block nanoparticle light absorption, though a recent study has implemented such schemes in light upconversion[16], and some work exploring the photochemical effects surface ligands have on lanthanide nanoparticle luminescence has been conducted[17–23].

In this report, we describe the construction of Eu-doped, rare-earth nanoparticles featuring a hydroxypyridinone (HOPO) ligand derivative, 3,4,3-LI(1,2-HOPO) (abbreviated '343'), as an ultraviolet photosensitizer. These constructs depart significantly from known systems such as dye-sensitized TiO_2 nanoparticles, where the stated purpose of photon absorption is generation of delocalized charge carriers, rather than the efficient production and radiative decay of lower-frequency excitons, the central focus of this work.

It has been previously shown that population of Eu(III) excited states in the Eu(III)-343 solution complex occur via energy transfer from the 343 triplet state following UV absorption by the ligand[24–27]. Surface display of this lanthanide chelator on nanoparticle surfaces is achieved through substitution of 1-oleate ligands retained on the nanoparticles following their initial synthesis. The resultant nanocrystals show good performance as UV → Vis converters, with red luminescence resulting from UV exposure serving as a diagnostic of Eu(III) sensitization by 343. Here, funneling light into europium ^5D_J manifolds via energy transfer from aromatic ligand absorbers benefits from the high molar absorptivity of 343 ($\varepsilon_{320\,nm}$ ~17,000 M^{-1} cm^{-1}) relative to f-f transitions. The net effect is an expansion of light absorption by over three orders of magnitude relative to typical lanthanide nanocrystals, where metal-centered excitation is generally employed, while dramatically improving peak luminescence relative to direct Eu excitation. As a consequence of 343's broad absorption profile, this scheme also significantly increases the spectral bandwidth available for nanoparticle light conversion, a notable improvement over the narrow absorption lines typical of lanthanides.

Absorption data acquired after the displacement of 1-oleate by 343 on nanocrystal surfaces reveal spectra representing the superposition of a broad ultraviolet transition (λ_{max} = 317 nm) and Rayleigh scattering. The spectral shape and transition energy of the UV absorption are characteristic of the 343 ligand and are not observed in the absorption spectra of the unmodified particles (Figure 1). Additionally, the normalized difference spectrum between the ligand-modified and unmodified particles looks virtually identical to that of the free ligand. Taken together, these data indicate that the 343 chelator effectively binds lanthanide ions at the surface of $NaGdF_4$ nanoparticles, as predicted from

the extremely high thermodynamic binding affinity of the ligand for trivalent lanthanide ions ($\log \beta_{Eu\text{-}343}$ = 20.2 and $\log \beta_{Gd\text{-}343}$ = 20.5)[26].

Emission spectra of Eu-doped, 343-modified nanocrystals dispersed in ethanol reveal a strong dependence of the Eu(III) luminescence on excitation in the ultraviolet region that is absent in the unmodified nanocrystals (Figure 2). Specifically, the $^5D_0 \rightarrow {}^7F_2$ Eu transition exhibits an excitation dependence reflective of the 343 absorption spectrum, with metal-centered emission observed at excitation wavelengths ranging from 300-360 nm and peaking around 340 nm (Figure 3). This correspondence between the nanoparticle action spectrum and the 343 absorption spectrum, along with concomitant Eu emission upon UV irradiation, demonstrates energy transfer between ligand and metal states is operative. This observation is consistent with previous reports describing Eu(III) sensitization by 343 phosphorescence in the Eu-343 molecular complex.[25] The absence of europium luminescence in no-343 and undoped $NaGdF_4$-3,4,3 controls upon UV excitation corroborate the interpretation that the red emission from these particles is dependent on ligand-to-metal energy transfer between 343 surface chelators and the Eu(III) lattice dopants. Probes of nanocrystal luminescence upon 464 nm europium excitation ($^7F_{0,1} \rightarrow {}^5D_2$ transition), with the same instrument parameters as used for UV ligand excitation, revealed a peak intensity at 612 nm (5×10^4 counts s^{-1}) four orders of magnitude smaller than the ligand-sensitized metal luminescence (2×10^8 counts s^{-1}; S.1), a dramatic improvement for this nanoparticle system. Previous studies of related systems have yielded substantially smaller luminescence enhancements, when reported[19,21].

The conditions used for achieving nanoparticle ligation allowed for the likelihood of particle surface etching, with aqueous Eu^{3+} and Gd^{3+} arising as potential byproducts. Such free ion formation would result in assembly of the Eu-343 solution complex during ligand incubations. It was therefore necessary to verify that the observed luminescence was genuine nanoparticle emission, as opposed to residual emission by the molecular complex. To test for this possibility, the final washes of all nanoparticles following ligand addition were saved and tested for Eu luminescence. Our data show that the free complex is indeed produced during the ligand addition. However, the luminescence intensity of the wash represents a minor fraction (< 0.0045) of the total emission signal after only four wash cycles (Figure 2, inset).

Overall sensitization efficiencies were evaluated through determination of nanoparticle external quantum yields using the integrated sphere method. Variability in syntheses between independent nanoparticle batches resulted in a quantum yield of 3.3 ± 0.6 %. To quantitatively determine the sources of non-radiative losses in this system, we use our findings to provide estimates of the ligand to metal energy transfer rate and efficiency. Our approach is rooted in first calculating the average energy transfer efficiency ($<\eta>$) through equation (1)[28]:

$$<\eta> = 1 - \sum_j \frac{\tau_{DAj}}{\tau_{Dj}} c_j \qquad (1),$$

To account for the multiple donor states arising from splitting of the 343 triplet, we present modifications of the typical rate and energy efficiency equations used for energy transfer. Here, an averaged energy transfer rate is comprised of a weighted summation of emissive state lifetimes according to their respective spectral contributions, where τ_{Dj} and τ_{DAj} are the respective lifetimes of the *j*th 343 triplet donor (D) levels in the absence and presence of the europium acceptor (A). The normalized coefficient, c_j. is used to represent the spectral contribution of individual states *j* to the overall transient decay. An average rate of energy transfer between ligand and metal states is then found according to equation (2):

$$\langle k_T \rangle = \frac{\langle \eta \rangle \langle k_D \rangle}{1 - \langle \eta \rangle} \quad (2).$$

Here, $\langle k_T \rangle$ is the averaged energy transfer rate, while $\langle k_D \rangle$, the expectation value for the 343 triplet decay rate in the absence of acceptor (Eu^{3+}) ion, is defined as:

$$\langle k_D \rangle = \sum_j k_{Dj} c_j \quad (3),$$

with k_{Dj} expressing the decay rate of the *j*th component of the 343 triplet.

Donor luminescence lifetimes in the presence and absence of europium acceptor quenching were quantified through time-resolved measurement of 343 phosphorescence from $NaGdF_4$-343 nanoparticles under 317 nm excitation at 77 K. Steady-state measurement of the 343 ligand at 77 K reveals a broad emission centered around 525 nm, assigned to the triplet, and a minor peak around 415 nm assigned to residual singlet luminescence (Figure 4). Monitoring the ligand triplet's decay at 525 nm yields a decay process composed of three distinct processes (S.2). Averaging data over three trials reveals that two of these three phases display significant quenching upon europium substitution, suggesting that these are states implicated in energy transfer between the ligand and metal. This conclusion is also supported by Gaussian deconvolution of the 343 triplet steady-state luminescence, which reveals two overlapping electronic contributions to the 525 nm emission signal used for time-dependent probes (Figure 4). Both components display decay constants in a range characteristic of triplet state deactivation and spectral overlap with the hypersensitive Eu^{3+} $^7F_{0,1} \rightarrow {}^5D_2$ absorption at 464 nm (S.1, S.2). In the undoped case, $k_1 = 1513 \pm 301\ s^{-1}$, and $k_3 = 29.7 \pm 3.9\ s^{-1}$, while for europium-incorporated particles, $k_1 = 2652 \pm 216\ s^{-1}$ and $k_3 = 47.5 \pm 9.1\ s^{-1}$. Europium substitution, at the low concentration used for this study, does not significantly perturb the relative contributions of the fast and slow phases to the transient decay. At this wavelength, we find that $f = 0.3$ and 0.1 for the fast and slow components, respectively (S.2). A third phase contributing to the time-resolved spectra is largely unchanged by the 5% europium substitution, displaying decay rates that are statistically equivalent between the samples and Eu-free controls ($k_2 = 238.6 \pm 8.8\ s^{-1}$ and $240.8 \pm 20.5\ s^{-1}$, respectively; $f = 0.6$). Such behavior suggests that this component is not responsible for energy transfer observed between ligand and metal states in this system.

Comparison of the calculated energy transfer rate with measured 343 excited state lifetimes provides insight into the origins of the low quantum yields observed with this pilot system. Workup of the relevant spectral data yields a mean energy transfer rate of $124\ s^{-1}$ and an energy transfer efficiency of 0.17 between the 343 triplet excited state and the europium ^5D_J manifold. This energy transfer rate is considerably lower than the weighted decay time measured for the 343 donor ($600\ s^{-1}$), indicating that ligand triplet-to-ground state deactivation is favored over energy transfer in this system. It should be emphasized that this value of the transfer efficiency is likely an upper bound in our system, as these values are derived from cryogenic measurements, temperatures where triplet decay through non-radiative decay paths would be reduced relative to luminescence quenching at room temperature. Regardless, these findings indicate that poor coupling between the 343 triplet and europium-centered states largely accounts for the energetic losses, and correspondingly low quantum yields, observed during metal sensitization in these nanocrystals. It is therefore clear, despite its remarkable brightness, that the system described here could be significantly optimized through improvements of the ligand/lanthanide coupling.

This work suggests ligand-sensitized nanoparticles may serve as a viable route through which

the constraints of solar spectrum/semiconductor band gap mismatch, and the low absorption cross-sections of lanthanides, may be overcome for solid-state systems. However, the characterizations presented in this work are largely fundamental in nature, and incorporation of this technology into any commercial solar capture device first requires practical studies on luminescence optimization of these nanoparticle chelates, particularly through their dependence on Eu content and ligand:nanoparticle ratios. Furthermore, having demonstrated the viability of this approach opens up the possibility of sensitizing rare-earth fluorides suited for transforming UV light into NIR emission, where Si photocurrent response is greatest. While the much-studied Pr^{3+}/Yb^{3+} and Tb^{3+}/Yb^{3+} couples provide intuitive starting points for this effort[2,29–31], previous work in our group has indicated that utilizing Pr^{3+}/Yb^{3+} co-substitution will require a ligand better-suited for Pr^{3+} sensitization, as 343 displays poor coupling with the praseodymium ^3P_j levels required for two-photon downconversion via Yb^{3+} ($^2F_{5/2} \rightarrow {}^2F_{7/2}$) luminescence[26]. Natural extensions of the system outlined here also include sensitizing curium-doped $NaGdF_4$ / $NaYF_4$ lattices, a concept inspired by earlier reports of a high quantum yield (~45%) in the Cm^{3+}-343 metal-ligand complex[32]. Such work is forthcoming.

Methods

Nanoparticle Synthesis

Nanoparticles were synthesized according to the methods of Wang et al[4]. Reaction compositions were 3.8 ml $Gd(CH_3CO_2)_3 \cdot xH_2O$ (Sigma-Aldrich), 200 µl $Eu(CH_3CO_2)_3 \cdot xH_2O$ (Sigma-Aldrich) in a solvent composition of 8 ml 1-oleic acid (Alfa Aesar) and 12 ml 1-octadecene (90%, Sigma-Aldrich).

Ligand Surface Functionalization

Aliquots (2 ml) of nanoparticles in cyclohexane were precipitated by addition of 2 ml of ethanol. Particles were pelleted via centrifugation at 13000 rpm for 5 minutes. The solvent was decanted and the pellets resuspended in 2 ml ethanol using sonication. Centrifugation was then repeated and the solvent removed. Fresh ethanol (2 ml) was used to resuspend the particles before their addition to a 10 ml round bottom flask. Afterwards, 1 ml of 75 mM 3,4,3-LI(1,2-HOPO) (Ash Stevens, Inc.) in pH 6.0 50 mM Hepes was added, and the reaction was capped. The mixture was stirred overnight at 75 °C, to promote ligand binding to the nanoparticles, and washed five times in ethanol using alternating centrifugation and sonication steps.

Transmission Electron Microscopy (TEM)

TEM images were collected on a JEOL JEM-2100 LaB6 microscope. Stock suspensions of nanoparticles in cyclohexane were diluted by 1/5 in ethanol and dropcast onto TEM grids. Samples were mounted onto a single-tilt sample holder. Images were collected using a high-tension voltage of 200 kV (112 µA beam current), with exposure times limited to 100 ms.

UV-Vis Spectroscopy

Absorption spectra were collected on a Molecular Devices SPECTRAmax Plus 384 UV-Vis spectrometer. Nanoparticle suspensions were formed in ethanol and scattering at 500 nm was measured. Samples were diluted appropriately so that their A_{500} values were approximately 0.3, an optical density yielding stable colloidal suspensions in this solvent. Absorption spectroscopy also provided a qualitative measurement of nanoparticle:surface ligand ratios, through comparison of scattering intensities (A_{500}) relative to the peak 343 absorption at 325 nm.

Steady-State Luminescence Spectroscopy

Steady-state luminescence spectra were acquired on a Jobin Yvon Horiba Fluorolog system. Luminescence spectra of nanoparticles were collected using a 317 nm excitation wavelength sourced from a xenon arc lamp, 1 nm excitation / 3 nm emission slit settings and 1.0 s integration times at 1 nm resolution. Due to the overlap of our emission window (550-750 nm) with the second-harmonic of our excitation beam, a 400 nm longpass filter (S.8) was placed between the sample and detector to remove beam-generated interference for all luminescence measurements. Excitation (action) spectra were collected by monitoring the $^5D_0 \rightarrow {}^7F_2$ transition at 612 nm using 1 nm slits for both excitation and emission monochromators and 1.0 s integration times at 1 nm resolution. Nanoparticle samples were prepared as dilute solutions in ethanol to ensure stability of the suspension over the course of data collection (A_{500} ~ 0.3; 0.1 mg ml^{-1}).

Determination of the triplet state of 3,4,3-LI(1,2-HOPO) was achieved through measurement of the 77 K spectrum of the Gd-343 metal-ligand complex (180 μM) and $NaGdF_4$-343 nanoparticles in ethanol. Spectra were acquired using parameters of 1 nm excitation / 3 nm emission slits, 317 nm excitation, 1.0 s integration times and a luminescence window spanning 325 to 750 nm. For emission wavelengths longer or exceeding 600 nm, the 400 nm long pass filter was again used to remove secondary harmonic noise originating from the excitation source.

Time-resolved Luminescence Spectroscopy

Donor luminescence lifetimes were acquired through measurement of the 343 phosphorescence decay rate at 77 K, using the Fluorolog system in time-resolved (MCS lifetime) mode. Excitation parameters were as follows: 317 nm excitation, 14 nm excitation bandpass; 525 nm observation, 1 nm emission bandpass; 10 μs channel^{-1} and 3000 channels sweep^{-1} (30.0 ms observation window). Time-resolved data were fit to multi-exponential decay functions in MATLAB with the minimum number of components needed to provide a zero residual (Supporting Information).

Quantum Yield Determination

External quantum yields were determined using an integrated sphere according to the methodology of de Mello et. al[33]. Our placement of a neutral density filter between the sphere's exit port and the PMT detector when measuring the excitation beam signals requires a small modification of de Mello's equation:

$$\Phi = f_{exc}\left[\frac{P_c - (1-A)P_b}{L_a A}\right] \quad ;$$

$$A = 1 - \frac{L_c}{L_b} \quad .$$

$P_{b,c}$ are the integrated Eu emission spectra acquired under the respective conditions of indirect and direct excitation in the sphere. $L_{a,b,c}$ represent the filtered, integrated excitation beam as measured for the respective cases of no sample, indirect sample excitation and direct sample excitation. The factor f_{exc} represents the fraction of excitation light transmitted by the filter. The filter's light transmission at 355 nm was determined through measurement of the lamp excitation beam at 355 nm with 1 nm excitation and emission slit settings at an 0.1 nm resolution in both the presence and absence of the

filter. A light transmission factor, calculated from the ratio of the integrated spectra of filtered to unfiltered light, was found to be 0.160 at 355 nm (S.4). The integrated sphere setup used for these experiments was benchmarked using quinine sulfate as a standard (literature value: $\Phi = 0.54$). Quinine sulfate standards (Sigma-Aldrich) were prepped as dilute solutions (peak absorption ~ 0.05) in 50 mM H_2SO_4. Five independent determinations gave $\Phi = 0.557 \pm .046$ (8.2% error; S.6).
Samples were made such that the particle scattering intensity at 500 nm was ~ 0.3 and the ligand absorption intensity at 355 nm fell in the approximate range of 0.01 - 0.07 (after subtracting light scatter contributions to the scatter intensity by using the ligand-free nanoparticles as a baseline). Instrument parameters were as follows: Eu emission spectra were collected using 1 nm slits for both excitation and emission, under 355 nm sample excitation and a 550-750 nm observation window at 1 nm spectral resolution. Quinine sulfate spectra were acquired similarly, with a 365-600 nm emission range. Lamp spectra at 355 nm were collected using both emission and excitation slits of 1 nm, an observation window from 350-358 nm, and 0.05 nm resolution. All spectra for quantum yield calculations were collected using 4.0 s signal integration times.
Corrections for quantum yield luminescence spectra consisted of two types: the subtraction of residual solvent autoluminescence and a response adjustment for any wavelength-dependent light transmission bias of the sphere. Subtractive corrections were done through acquisition of luminescence spectra using pure ethanol using the same excitation parameters as for the sample.
Spectral adjustments for wavelength-dependent response of the sphere were determined by measuring the luminescence spectra of either quinine sulfate (400-600 nm) or fluorescein isothiocyanate (FITC, Sigma-Aldrich) from 600-710 nm both inside and outside the integrated sphere. An empirical response function describing the integrated sphere's light transmission bias, r(λ), was then derived from the following relation:

$$r(\lambda) = \frac{S_{No\ Sphere}(\lambda)}{S_{sphere}(\lambda)} \quad ,$$

where S is the luminescence spectrum of quinine sulfate or FITC. Integrated sphere luminescence spectra were then corrected for sphere response through multiplication by r(λ).

Supporting Information

Detailed descriptions of f-f nanoparticle excitation, time-resolved luminescence, TEM imaging, optics characterizations and raw quantum yield data for both standards and samples can be found in the Supporting Information.

Acknowledgements

The authors would like to thank Fan Liu, Joseph Varghese and Akram Boukai for helpful comments during writing of this manuscript.
This work was supported by the U.S. Department of Energy, Office of Science, Office of Basic Energy Sciences, Chemical Sciences, Geosciences, and Biosciences Division at the Lawrence Berkeley National Laboratory under Contract DE-AC02-05CH11231. RJA is the recipient of a U.S. Department of Energy, Office of Science Early Career Award.

306 **References**

(1) Shockley, W.; Queisser, H. J. Detailed Balance Limit of Efficiency of P-n Junction Solar Cells. *J. Appl. Phys.* **1961**, *32* (3), 510–519.

(2) Ende, B. M. van der; Aarts, L.; Meijerink, A. Lanthanide Ions as Spectral Converters for Solar Cells. *Phys. Chem. Chem. Phys.* **2009**, *11* (47), 11081–11095.

(3) Liu, C.; Wang, H.; Zhang, X.; Chen, D. Morphology- and Phase-Controlled Synthesis of Monodisperse Lanthanide-Doped NaGdF4 nanocrystals with Multicolor Photoluminescence. *J. Mater. Chem.* **2009**, *19* (4), 489–496.

(4) Wang, F.; Deng, R.; Liu, X. Preparation of Core-Shell NaGdF4 Nanoparticles Doped with Luminescent Lanthanide Ions to Be Used as Upconversion-Based Probes. *Nat. Protoc.* **2014**, *9* (7), 1634–1644.

(5) Li, X.; Wang, R.; Zhang, F.; Zhao, D. Engineering Homogeneous Doping in Single Nanoparticle To Enhance Upconversion Efficiency. *Nano Lett.* **2014**, *14* (6), 3634–3639.

(6) Jang, H. S.; Woo, K.; Lim, K. Bright Dual-Mode Green Emission from Selective Set of Dopant Ions in β-Na(Y,Gd)F4:Yb, Er/β-NaGdF4:Ce,Tb Core/shell Nanocrystals. *Opt. Express* **2012**, *20* (15), 17107.

(7) Wang, Z.-L.; Hao, J. H.; Chan, H. L. W. Down- and up-Conversion Photoluminescence, Cathodoluminescence and Paramagnetic Properties of NaGdF4:Yb^{3+}, Er^{3+} Submicron Disks Assembled from Primary Nanocrystals. *J. Mater. Chem.* **2010**, *20* (16), 3178–3185.

(8) Zhu, W.; Chen, D.; Lei, L.; Xu, J.; Wang, Y. An Active-Core/active-Shell Structure with Enhanced Quantum-Cutting Luminescence in Pr–Yb Co-Doped Monodisperse Nanoparticles. *Nanoscale* **2014**, *6* (18), 10500–10504.

(9) Mimun, L. C.; Ajithkumar, G.; Pokhrel, M.; Yust, B. G.; Elliott, Z. G.; Pedraza, F.; Dhanale, A.; Tang, L.; Lin, A.-L.; Dravid, V. P.; Sardar, D. K. Bimodal Imaging Using Neodymium Doped Gadolinium Fluoride Nanocrystals with near-Infrared to near-Infrared Downconversion Luminescence and Magnetic Resonance Properties. *J. Mater. Chem. B* **2013**, *1* (41), 5702.

(10) Chen, G.; Ohulchanskyy, T. Y.; Liu, S.; Law, W.-C.; Wu, F.; Swihart, M. T.; Ågren, H.; Prasad, P. N. Core/Shell NaGdF4:Nd^{3+}/NaGdF4 Nanocrystals with Efficient Near-Infrared to Near-Infrared Downconversion Photoluminescence for Bioimaging Applications. *ACS Nano* **2012**, *6* (4), 2969–2977.

(11) Ye, S.; Zhu, B.; Luo, J.; Chen, J.; Lakshminarayana, G.; Qiu, J. Enhanced Cooperative Quantum Cutting in Tm^{3+}- Yb^{3+} Codoped Glass Ceramics Containing LaF3 Nanocrystals. *Opt. Express* **2008**, *16* (12), 8989.

(12) Li, X.; Wang, R.; Zhang, F.; Zhou, L.; Shen, D.; Yao, C.; Zhao, D. Nd^{3+} Sensitized Up/Down Converting Dual-Mode Nanomaterials for Efficient In-Vitro and In-Vivo Bioimaging Excited at 800 Nm. *Sci. Rep.* **2013**, *3*.

(13) Bünzli, J.-C. G.; Piguet, C. Taking Advantage of Luminescent Lanthanide Ions. *Chem. Soc. Rev.* **2005**, *34* (12), 1048.

(14) Bünzli, J.-C. G. Lanthanide Luminescence for Biomedical Analyses and Imaging. *Chem. Rev.* **2010**, *110* (5), 2729–2755.

(15) Li, C.; Song, Z.; Li, Y.; Lou, K.; Qiu, J.; Yang, Z.; Yin, Z.; Wang, X.; Wang, Q.; Wan, R. Enhanced NIR Downconversion Luminescence by Precipitating Nano Ca5(PO4)3F Crystals in Eu^{2+}–Yb^{3+} Co-Doped Glass. *Spectrochim. Acta. A. Mol. Biomol. Spectrosc.* **2013**, *114*, 575–578.

(16) Zou, W.; Visser, C.; Maduro, J. A.; Pshenichnikov, M. S.; Hummelen, J. C. Broadband Dye-Sensitized Upconversion of near-Infrared Light. *Nat. Photonics* **2012**, *6* (8), 560–564.

(17) Banski, M.; Podhorodecki, A.; Misiewicz, J. NaYF4 Nanocrystals with TOPO Ligands: Synthesis-Dependent Structural and Luminescent Properties. *Phys. Chem. Chem. Phys.* **2013**, *15* (44), 19232–19241.

(18) Wawrzynczyk, D.; Bednarkiewicz, A.; Nyk, M.; Strek, W.; Samoc, M. Ligand-Dependent Luminescence of Ultra-Small Eu^{3+}-Doped NaYF4 Nanoparticles. *J. Nanoparticle Res.* **2013**, *15* (6) 1-11.

(19) Charbonnière, L. J.; Rehspringer, J.-L.; Ziessel, R.; Zimmermann, Y. Highly Luminescent Water-Soluble Lanthanide Nanoparticles through Surface Coating Sensitization. *New J. Chem.* **2008**, *32* (6), 1055–1059.

(20) Li, S. W.; Ren, H. J.; Ju, S. G. Sensitized Luminescence of LaF3:Eu^{3+} Nanoparticles through Pyromellitic Acid. *J. Nanosci. Nanotechnol.* **2014**, *14* (5), 3677–3682.

(21) Irfanullah, M.; Sharma, D. K.; Chulliyil, R.; Chowdhury, A. Europium-Doped LaF3 Nanocrystals with Organic 9-Oxidophenalenone Capping Ligands That Display Visible Light Excitable Steady-State Blue and Time-Delayed Red Emission. *Dalton Trans.* **2015**, *44* (7), 3082–3091.

(22) Janssens, S.; Williams, G. V. M.; Clarke, D. Systematic Study of Sensitized LaF3:Eu^{3+} Nanoparticles. *J. Appl. Phys.* **2011**, *109* (2), 023506.

(23) Zhang, J.; Shade, C. M.; Chengelis, D. A.; Petoud, S. A Strategy to Protect and Sensitize Near-Infrared Luminescent Nd3+ and Yb3+: Organic Tropolonate Ligands for the Sensitization of Ln3+-Doped NaYF4 Nanocrystals. *J. Am. Chem. Soc.* **2007**, *129* (48), 14834–14835.

(24) Moore, E. G.; Jocher, C. J.; Xu, J.; Werner, E. J.; Raymond, K. N. An Octadentate Luminescent Eu(III) 1,2-HOPO Chelate with Potent Aqueous Stability. *Inorg. Chem.* **2007**, *46* (14), 5468–5470.

(25) Abergel, R. J.; D'Aléo, A.; Ng Pak Leung, C.; Shuh, D. K.; Raymond, K. N. Using the Antenna Effect as a Spectroscopic Tool: Photophysics and Solution Thermodynamics of the Model Luminescent Hydroxypyridonate Complex [EuIII(3,4,3-LI(1,2-HOPO))]−. *Inorg. Chem.* **2009**,

48 (23), 10868–10870.

(26) Sturzbecher-Hoehne, M.; Ng Pak Leung, C.; D'Aléo, A.; Kullgren, B.; Prigent, A.-L.; Shuh, D. K.; Raymond, K. N.; Abergel, R. J. 3,4,3-LI(1,2-HOPO): In Vitro Formation of Highly Stable Lanthanide Complexes Translates into Efficacious in Vivo Europium Decorporation. *Dalton Trans.* **2011**, *40* (33), 8340.

(27) Daumann, L. J.; Tatum, D. S.; Snyder, B. E. R.; Ni, C.; Law, G.; Solomon, E. I.; Raymond, K. N. New Insights into Structure and Luminescence of EuIII and SmIII Complexes of the 3,4,3-LI(1,2-HOPO) Ligand. *J. Am. Chem. Soc.* **2015**, *137* (8), 2816–2819.

(28) *Principles of Fluorescence Spectroscopy*; Lakowicz, J. R., Ed.; Springer US: Boston, MA, 2006.

(29) Lakshminarayana, G.; Yang, H.; Ye, S.; Liu, Y.; Qiu, J. Cooperative Downconversion Luminescence in Pr^{3+}/Yb^{3+}:SiO2–Al2O3–BaF2–GdF3 Glasses. *J. Mater. Res.* **2008**, *23* (11), 3090–3095.

(30) van Wijngaarden, J. T.; Scheidelaar, S.; Vlugt, T. J. H.; Reid, M. F.; Meijerink, A. Energy Transfer Mechanism for Downconversion in the (Pr^{3+}, Yb^{3+}) Couple. *Phys. Rev. B* **2010**, *81* (15), 155112.

(31) Ye, S.; Katayama, Y.; Tanabe, S. Down Conversion Luminescence of Tb^{3+}–Yb^{3+} Codoped SrF2 Precipitated Glass Ceramics. *J. Non-Cryst. Solids* **2011**, *357* (11–13), 2268–2271.

(32) Sturzbecher-Hoehne, M.; Kullgren, B.; Jarvis, E. E.; An, D. D.; Abergel, R. J. Highly Luminescent and Stable Hydroxypyridinonate Complexes: A Step Towards New Curium Decontamination Strategies. *Chem. – Eur. J.* **2014**, *20* (32), 9962–9968.

(33) de Mello, J. C.; Wittmann, H. F.; Friend, R. H. An Improved Experimental Determination of External Photoluminescence Quantum Efficiency. *Adv. Mater.* **1997**, *9* (3), 230–232.

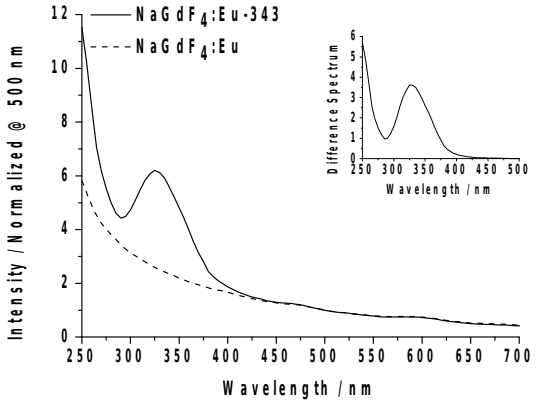

309 **Figure 1.** Absorption spectra of $NaGd_{0.95}Eu_{0.05}F_4$ nanoparticles with and without
310 3,4,3-LI(1,2-HOPO) surface modification suspended in ethanol. Inset: difference
311 spectrum between modified and unmodified nanoparticles.

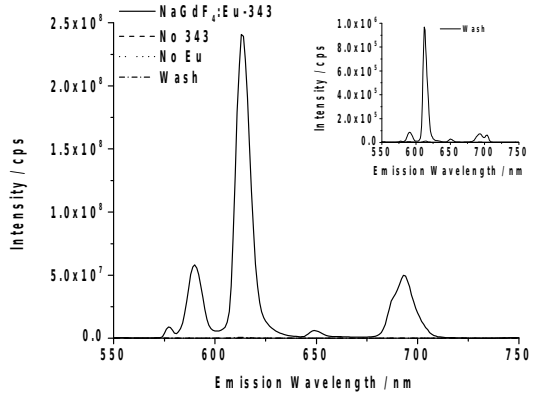

312

313 **Figure 2.** Nanoparticle luminescence spectra. Nanoparticles featuring 343
314 surface ligands (solid) display intense europium emission upon UV irradiation (λ_{exc}
315 = 317 nm); excitation of unmodified, europium-doped nanoparticles (dash) and
316 undoped nanoparticles containing 343 (dot) result in no observable luminescence
317 under those same conditions (dilute suspensions in ethanol, $A_{500} \sim 0.3$; 0.1 mg ml^{-1}).
318 Inset: magnified view of wash spectra in ethanol, with Eu-free and ligand-free
319 controls still resulting in no observable signal on that scale.

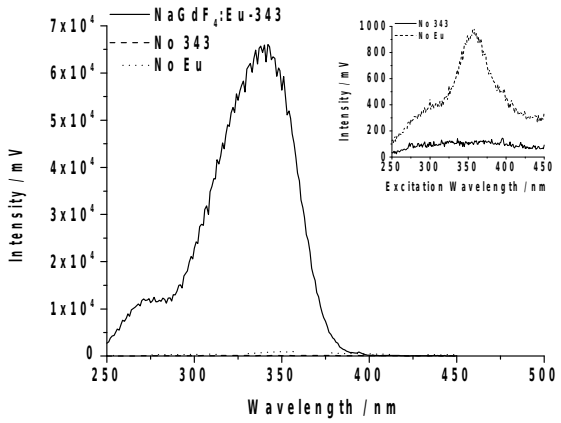

Figure 3. Nanoparticle excitation (action) spectra in ethanol measured at 612 nm. The broadness of the 343 absorption spectrum results in a nanoparticle action spectrum with a spectral bandwidth significantly greater than those of the narrow transitions typical of lanthanides. The minor peak seen in no-Eu control (inset, magnified scale) is a result of broad luminescence from the broad 343 emission, which has residual overlap with the Eu luminescence region.

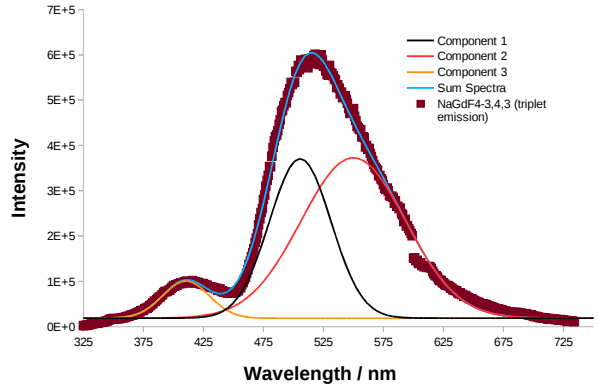

Figure 4. Emission spectrum (λ_{exc} = 317 nm) of 3,4,3-LI(1,2-HOPO) (bound to control nanoparticles as $NaGdF_4$-343) in ethanol at 77 K (red squares). The peak emission around 525 nm is a composition of states (components 1 & 2) which comprise the 343 triplet manifold. The Gaussian character of these deconvoluted states suggests a significant degree of heterogeneous broadening in the ligand luminescence. Overlap of multiple components at 525 nm provides a physical basis for the observed multi-exponential character of time-resolved probes at this wavelength.

Table of Contents Graphic